Fall Technical Meeting
of the Western States Section of the Combustion Institute
Hosted by the University of California at Irvine
Oct 27-28, 2009

Characterization of Freely Propagating Hydrogen Flames

Xinfeng Gao[1,†], *Marcus S. Day*[1] *and John B. Bell*[1]

[1] *Lawrence Berkeley National Laboratory, Berkeley, CA 94720, USA*
[†] *Corresponding author: XinfengGao@lbl.gov*

We explore the detailed structure of heat release and the energy budget for a freely-propagating lean, premixed hydrogen flame. At lean conditions, the flame is thermodiffusively unstable and spontaneously develops the cellular burning structures, characteristic of this type of flame. The instabilities in the system saturate quickly, resulting in robust, slowly evolving cellular burning features. In the simulations, we employ a feedback control strategy to stabilize the mean location of the evolving flame so that in the computational domain the flame is statisically stationary, allowing us to collect data for analysis. To analyze the local flame structure we identify the flame surface with an isotherm and construct a local coordinate system around the flame by following integral curves of the temperature gradient. We extract local heat release along these integral curves as we trace along the flame surface. We compare these local heat release profiles with heat release profiles from flat laminar flames over a range of equivalence ratios and show that the heat release profiles in the two-dimensional flame are well matched by the laminar profiles. We also examine the energy budget along integral curves through the flame and compare to the flat laminar flame. From a flat, laminar flame simulation we also identify the dominant reactions contributing to the heat release and analyze their behavior in local flame coordinates. Finally, we explore how the features of the heat release profiles correlate with flame curvature.

1. Introduction

With the increasingly stringent emission regulations imposed by governments worldwide and a desire to reduce dependence on petroleum-based fuels, there is considerable interest in the combusion community on the development lean, premixed combustion systems that can burn alternative fuels including hydrogen or a mixture of hydrogen and another combustible gas (methane, carbon monoxide, natural gas). However, the feasibility of lean premixed fuel-flexible systems depends on the development of robust flame stabilization techniques. Development of these types of

systems relies on a thorough understanding of flame propagation, particularly, for the case of hydrogen-rich fuels where thermo-diffusive instabilities can have significant impact on the overall flame dynamics. In this study, we analyze a freely propagating premixed hydrogen flame with equilvalence ratio, $\phi = 0.37$, focusing on the structure of the heat release and how it is effected by the thermodiffusive instability.

This paper is structured as follows. In Section 2, the computational methodology and numerical algorithm for solving low Mach number combusting flows are summarized. Details of the simulation are briefly discussed in Section 3. In Section 4, we first discuss the structure of the $\phi = 0.37$ flat laminar flame, which we will subsequently use as a baseline for discussing the freely propagating flame. Finally, some conclusions are drawn in Section 5.

2. Computational Methodology and Numerical Algorithm

The simulations presented here are based on a low Mach number formulation of the reacting flow equations. The methodology treats the fluid as a mixture of perfect gases. We use a mixture-averaged model for differential species diffusion and ignore Soret, Dufour, gravity and radiative transport processes. With these assumptions, the system of low Mach number flow equations for an open domain is

$$\frac{\partial \rho U}{\partial t} + \nabla \cdot \rho UU = -\nabla \pi + \nabla \cdot \tau, \tag{1}$$

$$\frac{\partial \rho Y_m}{\partial t} + \nabla \cdot U \rho Y_m = \nabla \cdot \rho D_m \nabla Y_m - \dot{\omega}_m, \tag{2}$$

$$\frac{\partial \rho h}{\partial t} + \nabla \cdot U \rho h = \nabla \cdot \frac{\lambda}{c_p} \nabla h + \sum_m \nabla \cdot h_m \Big(\rho D_m - \frac{\lambda}{c_p} \Big) \nabla Y_m, \tag{3}$$

where ρ is the gas mixture density, U is the gas mixture velocity, Y_m is the mass fraction of species m, h is the mass-weighted enthalpy of the gas mixture, T is the mixture temperature, and $\dot{\omega}_m$ is the net destruction rate for species m due to chemical reactions. In addition, λ is the thermal conductivity, τ is the stress tensor, c_p is the specific heat of the mixture, and $h_m(T)$ and D_m are the enthalpy and species mixture-averaged diffusion coefficients of species m, respectively. These evolution equations are supplemented by an equation of state for a perfect gas mixture:

$$p_0 = \rho R_{mix} T = \rho \mathcal{R} T \sum_m \frac{Y_m}{W_m}$$

where W_m is the molecular mass of species m, and $\mathcal{R}$ is the universal gas constant. Additionally, π is the perturbational pressure field ($\pi/p_0 \sim \mathcal{O}(M^2)$), where M is the Mach number. All thermodynamic quantities are independent of π. In the low Mach number model, the equation of state constrains the evolution and removes acoustic wave propagation from the dynamics of the system. We use the hydrogen submechanism from GRI-Mech 2.11, which includes 9 species and 27 reactions, to describe the kinetics, thermodynamics and transport properties.

The basic discretization combines a symmetric operator-split treatment of chemistry and transport with a density-weighted approximate projection method. The projection method incorporates the constraint by imposing a constraint on the velocity divergence that forces the evolution to satisfy the equation of state. The resulting integration of the advective terms proceeds on the time scale of the relatively slow advective transport. Faster diffusion and chemistry processes are treated time-implicitly. This integration scheme is embedded in a parallel adaptive mesh refinement algorithm framework based on a hierarchical system of rectangular grid patches. The complete integration algorithm is second-order accurate in both space and time, and discretely conserves species mass and enthalpy. The reader is referred to [1] for details of the low Mach number model and its numerical implementation and to [2–9] for previous applications of this methodology to the simulation of premixed flames.

3. Numerical Solution-Convergence Analysis

The flow configuration we consider initializes a flat laminar flame in a square domain, 8cm $\times$ 8cm, oriented so that the flame propagates downward. Since no gravitational force is included, up and down are for orientation only. A cold fuel-air premixture enters the domain through bottom boundary, and hot combustion products exit the domain through the top. The other computational boundary is periodic. We use a feeback control algorithm, introduced in Bell et al. [4], that automatically adjusts the inflow rate at the bottom boundary to hold the flame at a fixed location in the domain, in this case, 3 cm. (See [4] for additional details and a demonstration of the efficacy of the control algorithm applied to premixed flames.)

We simulated a two-dimensional freely-propagating premixed H_2 flame. The simulation was run until the flame was stabilized, after which statistics were gathered from the subsequent evolution. A specific flame marker, H, was used as a indicator during adaptive mesh refinement for flame simulations. This measure was found to provide reliable detection of flame fronts and combustion zones. To ensure that the data accurately represents the flame, we performed convergence analysis that showed that a spatial resolution of $39\mu m$ was adequate to resolve the flame, consistent with results in a previous study [2].

4. Flame Analysis

4.1. Steady Flat Hydrogen Flame

Fukutani [10] studied the detailed structure of heat release in a stoichiometric hydrogen flame. That work identified six predominant reactions

$$\mathrm{R}_2: \ \mathrm{H} + \mathrm{O}_2 \Leftrightarrow \mathrm{O} + \mathrm{OH} \tag{4}$$

$$\mathrm{R}_3: \ \mathrm{O} + \mathrm{H}_2 \Leftrightarrow \mathrm{H} + \mathrm{OH} \tag{5}$$

$$\mathrm{R}_5: \ \mathrm{OH} + \mathrm{H}_2 \Leftrightarrow \mathrm{H} + \mathrm{H_2O} \tag{6}$$

$$\mathrm{R}_{10}: \mathrm{H} + \mathrm{O}_2 + \mathrm{M} \Leftrightarrow \mathrm{HO}_2 + \mathrm{M} \tag{7}$$

$$\mathrm{R}_{11}: \mathrm{H} + \mathrm{HO}_2 \Leftrightarrow \mathrm{O}_2 + \mathrm{H}_2 \tag{8}$$

$$\mathrm{R}_{12}: \mathrm{H} + \mathrm{HO}_2 \Leftrightarrow 2\mathrm{OH}\,. \tag{9}$$

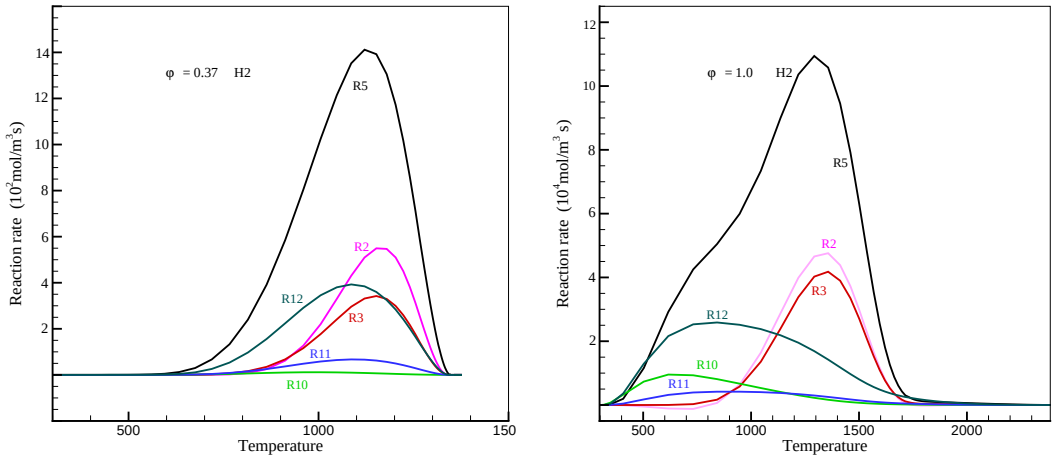

(a) lean $\phi = 0.37$ H_2 flame (b) stoichiometric H_2 flame

Fig. 1: Reaction rates for reactions R_2, R_3, R_5, R_{10}, R_{11} and R_{12} for both stoichiometric and lean premixed hydrogen flames.

that were responsible for most of the heat release in the flame. (We have retained the same reaction numbers as those used by Fukutani.)

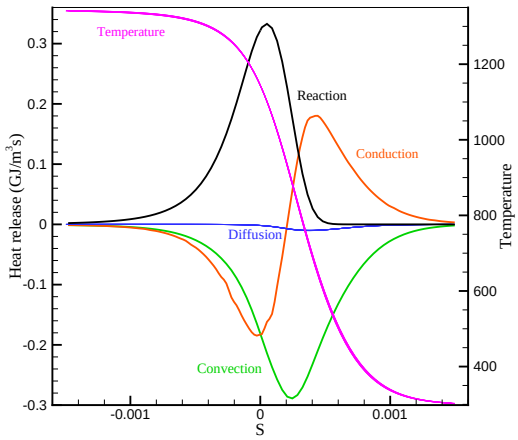

Fig. 2: Heat release rates due to convection, conduction, diffusion and chemical reaction for lean H_2 flames.

In Figures 1(a) and 1(b) we plot the reaction rates for each of those reactions for a lean $\phi = 0.37$ premixed flame and, for comparison, the stoichiometric flame. We note that for the lean flame the intensity of the reactions is reduced by approximately two orders of magnitude. We also note that in the lean case there is a dramatic reduction in the amount of reaction that occurs on the low temperature side of the flame. The low temperature reactions rely on the presence of a pool of H formed in the reaction zone and diffused into the low temperature region, which is not available for the lean flame [11, 12]. As a result, R_{10} and R_{11} no longer play a key role in the heat release at lean conditions.

From the governing equations, we can derive an auxiliary equation for temperature given by

$$\rho C_{p_{\text{mix}}}\left(\frac{\partial T}{\partial t} + U \cdot \nabla T\right) = \nabla \cdot \lambda \nabla T + \sum_m \rho D_m \nabla h_m(T) \cdot \nabla Y_m + \sum_m \dot{\omega_m} h_m(T) \quad (10)$$

Using Eq. (10) we can identify terms in the energy balance due to the convection, con-

duction, diffusion (heat transfer accompanying species diffusion process), and chemical reactions, which are plotted in Figure 2. We note that the crossover point at which the reaction term becomes larger than the conduction term shifts to 830K for the lean flame, compared to 450K for the stoichiometric flame, as reported by Fukutani [10], which reflects the reduced pool of available radicals in the lean flame.

4.2. Freely-Propagating Lean Hydrogen Flames

Our goal is to quantify how the cellular burning pattern associated with the thermodiffusively unstable lean premixed hydrogen flame affects the heat release of the flame. Figure 3 illustrates the freely propagating flame showing the heat release rate and the temperature field. The images show the cellular burning structures, where the fuel consumption and heat release are highly variable along the "flame surface". In particular, in regions of high positive curvature, we see an intensification of heat release and pockets of higher post-flame temperature, indicated by darker red in the figure.

To analyze this local intensification of heat release in greater detail, we construct a local coordinate system around the flame. We first identify the flame with the $T = 1144$ isotherm, corresponding the the temperature where the maximum heat release occurs in the flat laminar flame. (We note that in the gaps in the flame seen in Figure 3, there is essentially no burning and what one means a flame surface is somewhat ill-defined.) We then extend along integral curves of ∇T to define a local orthogonal coordinate system as illustrated in Figure 4,

We evaluated the terms of the energy balance due to convection, conduction, diffusion (heat transfer accompanying differential species diffusion) and chemical reactions along each of the control volumes defined by the local coordinate system as shown in Figure 4, The energy budget for each control volume at a particular time step is shown in Figure 5. The profiles show considerable variability with reaction and conduction terms rising to 3-4 times their laminar values. In Figure 6 we extract heat release as a function of temperature in each of the control volumes in the local coordinate system. In the image we also plot the heat release as a function of temperature for flat, unstretched laminar flames over a range of equivalence ratios. The curves from the freely propagating flame closely match the laminar flame data for the more intensely burning parts of flame. This suggests that the regions of intense burning can be well-approximated by laminar flames that have been enriched by preferential diffusion of molecular hydrogen into the cold region of the flame. In the weakly burning portion of the flame where the integrated heat release is reduced, although the trends are similar, the agreement is not as good. In particular, the heat release profiles for $\phi < 0.37$ decay more sharply at higher temperatures than the data from the freely propagating flame, suggesting some type of multidimensional diffusive mechanisms for maintaining the heat release in the freely propagating flame.

In the laminar $\phi = 0.37$ flame, four reactions, R_2, R_3, R_5 and R_{12} were found to account for the bulk of the heat release in the flame. Figure 7 compares the distributions of these four reaction rates in temperature space over the control volumes

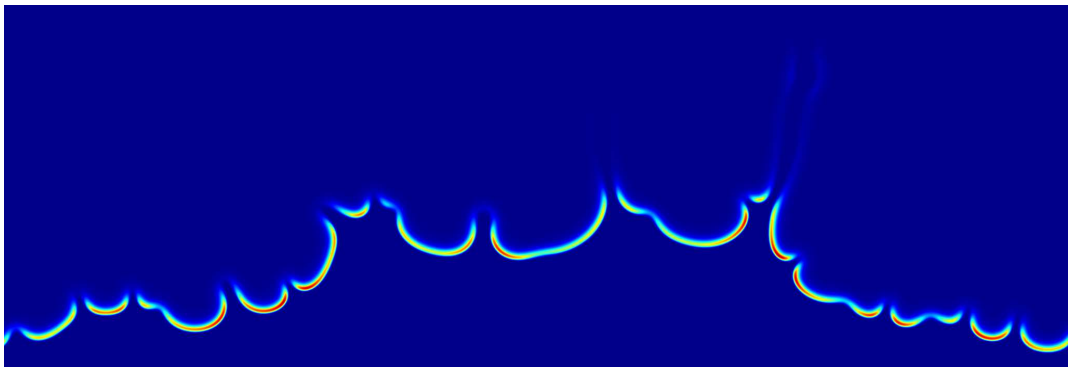

(a) Heat release field

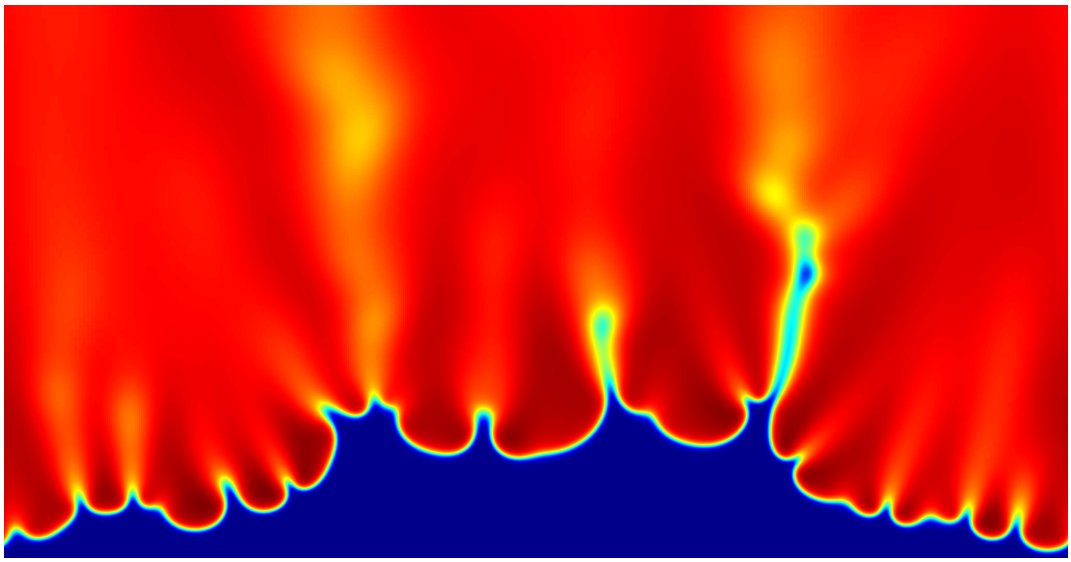

(b) Temperature field

Fig. 3: The freely propagating flame images show the fields of heat release rates and temperature, respectively.

in Figure 4. In each figure, the color map is based on the integral heat release rate over the control volumes. The relative strength of each of the reactions correlates well with the integrate heat release and shapes are similar to the laminar flame. These observations indicate that the chemical pathways in the flame are remaining relatively unchanged; all that is changing is the relative intensity of the burning.

To relate the variability in heat release to the local flame structure, we present, in Figure 8, a scatter plot of local heat release integrated over a control volume versus local flame curvature. The image shows a very strong positive curvature, quantifying the relationship observed in the flame image, Figure 3. By integrating local fuel consumption instead of heat release we can, after suitable normalization, define a fuel-consumption based local flame speed, s_c^{loc}. In Figure 9 we plot s_c^{loc} normalized by the laminar flame speed versus curvature. The data is almost identifical to the heat

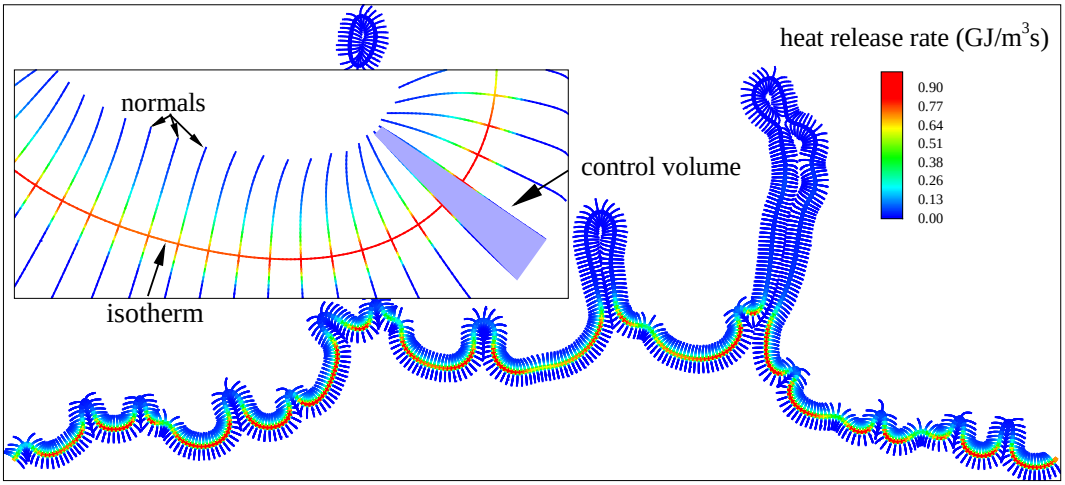

Fig. 4: Illustration of an isotherm (T = 1144 K) for the freely propagating flame.

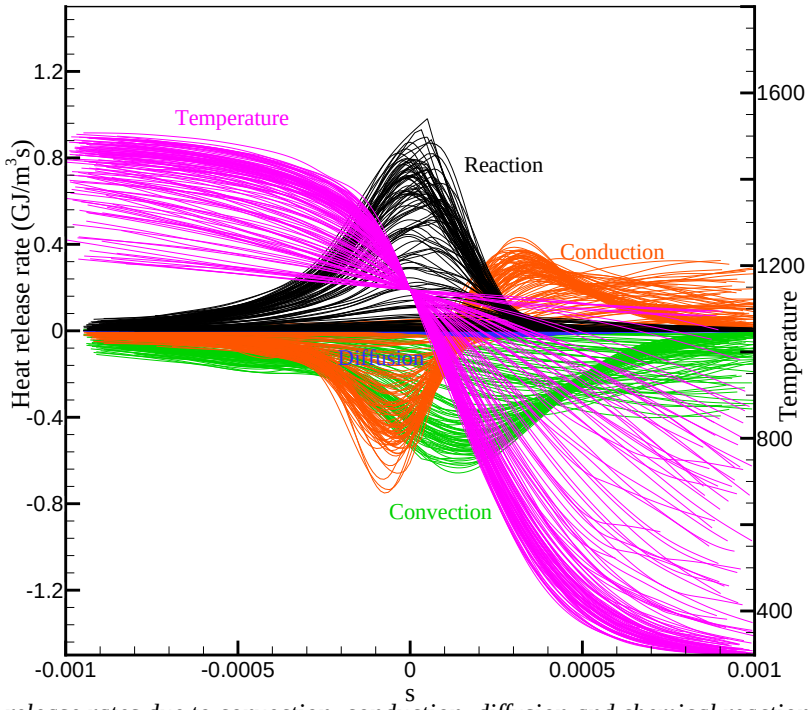

Fig. 5: Heat release rates due to convection, conduction, diffusion and chemical reaction for the freely propagating flame.

release data in Figure 8 showing that heat release and local consumption are tightly coupled. The strong correlation between local flame speeds and positive curvature reflects a negative Markstein number, indicating the thermo-diffusive instability of freely propagating hydrogen flames with local speeds as high as 2.5 times the laminar flame value.

5. Conclusions

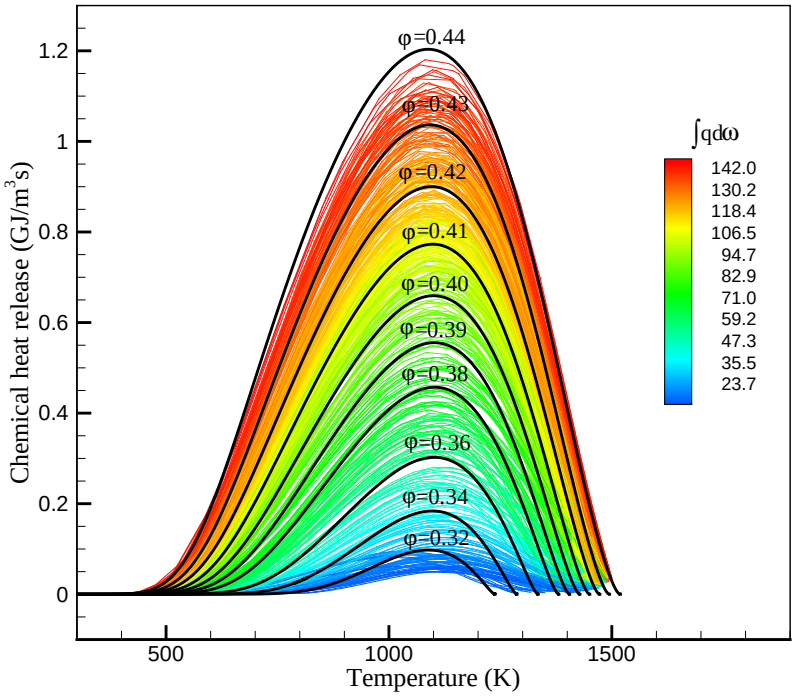

Fig. 6: Comparisons of distributions of chemical heat release rates between the freely propagating and the flat flames.

We have examined the structure of the heat release in a freely propagating premixed flame at $\phi = 0.37$. The simulation shows dramatic enhancements in local heat release in regions of positive curvature. In the regions where the heat release is enhanced, the heat release as a function of temperature is well-approximated by the heat release of enriched laminar flames, suggesting that preferential diffusion is locally enriching the cold side of the flame with additional fuel. Examining the specific reactions that play a significant role in heat release we see that they all essentially scale with the overall local heat release so that the variation along the flame front can be described by a single parameter. Furthermore, we find that both the integrated heat release and local consumption-based flame speed correlate strongly with curvature. These observations have potential use in developing suitable turbulence chemistry interaction models for lean premixed H_2 flames.

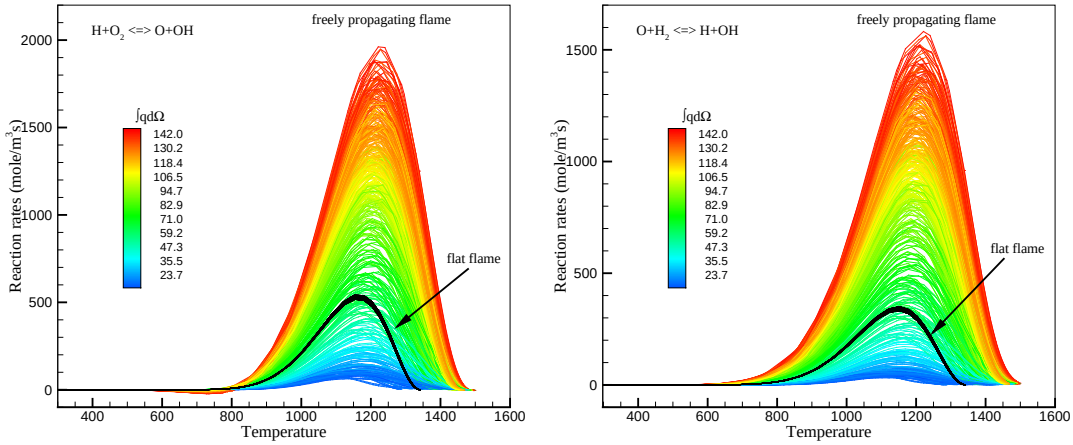

(a) R_2: $H+O_2 \Leftrightarrow O+OH$

(b) R_3: $O+H_2 \Leftrightarrow H+OH$

(c) R_5: $OH+H_2 \Leftrightarrow H+H_2O$

(d) R_{12}: $H+HO_2 \Leftrightarrow 2OH$

Fig. 7: Comparisons of distributions of reaction rates in temperature space between freely propagating and flat H_2 flames.

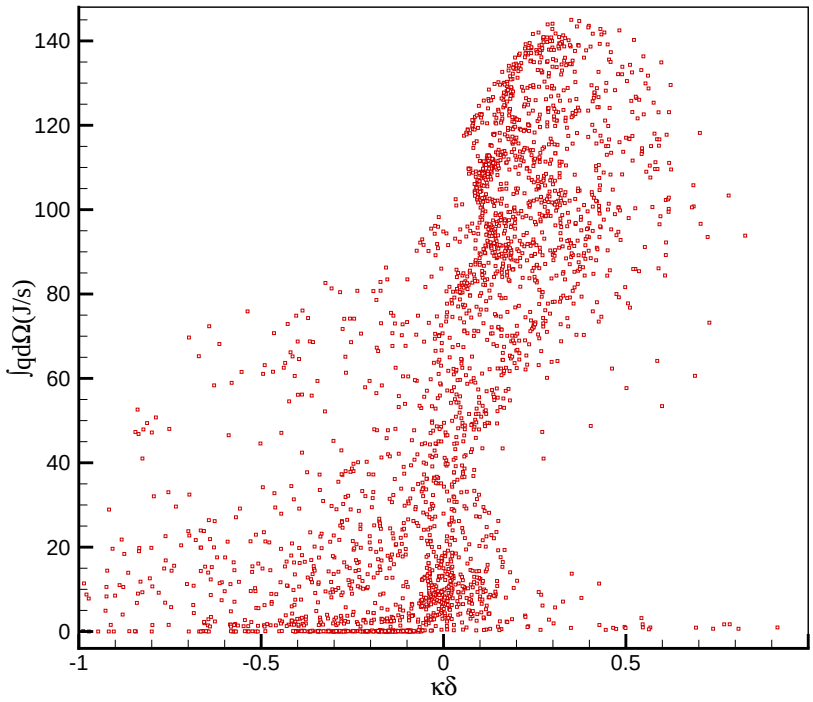

Fig. 8: Correlations of the integrated heat release rates (over control volumes) with the normalized curvature.

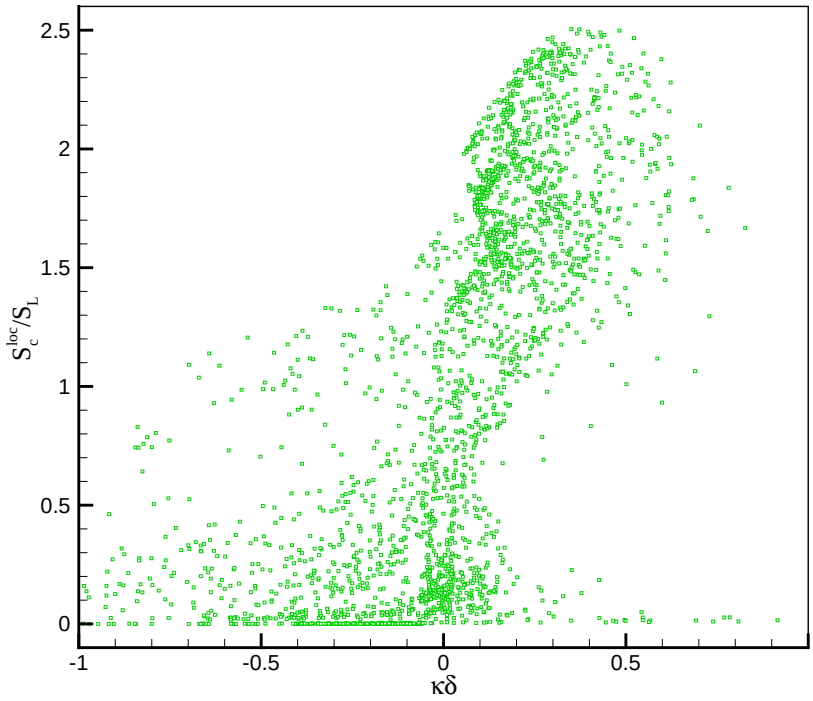

Fig. 9: Correlations of local flame speeds with the normalized curvature.

References

[1] M. S. Day, J. B. Bell, *Combust. Theory Modelling* 4 (2000) 535–556.

[2] J. B. Bell, R. K. Cheng, M. S. Day, I. G. Shepherd, *Proc. Combust. Inst.* 31 (2007) 1309–1317.

[3] J. B. Bell, M. S. Day, J. F. Grcar, *Proc. Combust. Inst.* 29 (2002) 1987–1993.

[4] J. B. Bell, M. S. Day, J. F. Grcar, M. J. Lijewski, *Comm. App. Math. Comput. Sci.* 1 (1) (2005) 29–52.

[5] M. S. Day, J. B. Bell, P.-T. Bremer, V. Pascucci, V. Beckner, M. Lijewski, *Combust. Flame* 156 (2009) 1035–1045.

[6] J. B. Bell, M. S. Day, A. S. Almgren, M. J. Lijewski, C. A. Rendleman, R. K. Cheng, I. G. Shepherd, *Simulation of Lean Premixed Turbulent Combustion*, Vol. 46 of *Journal of Physics Conference Series: SciDAC 2006 (W. Tang, Ed.)*, Institute of Physics Publishing, Denver, CO, 2006.

[7] J. B. Bell, M. S. Day, I. G. Shepherd, M. Johnson, R. K. Cheng, J. F. Grcar, V. E. Beckner, M. J. Lijewski, *Proc. Natl. Acad. Sci. USA* 102 (29) (2005) 10006–10011.

[8] J. B. Bell, M. S. Day, J. F. Grcar, M. J. Lijewski, J. F. Driscoll, S. F. Filatyev, *Proc. Combust. Inst.* 31 (2007) 1299–1307.

[9] J. B. Bell, M. S. Day, J. F. Grcar, M. J. Lijewski, in: P. Wessleing, E. Onate, J. Périaux (Eds.), Proceedings of the European Conference on Computational Fluid Dynamics, Egmond Aan Zee, The Netherlands, 2006, pp. 432:1–19, 5–8 September.

[10] S. Fukutani, N. Kunioshi, H. Jinno, *Bull. Chem. Soc. Jpn.* 63 (1990) 2191–2198.

[11] M. J. Day, G. Dixon-Lewis, K. Thoomson, *Proc. Roy. Soc. London Ser. A* 330 (1972) 199–218, issue 1581.

[12] G. Dixon-Lewis, G. L. Isles, R. Walmsley, *Proc. Roy. Soc. London Ser. A* 331 (1973) 571–584.